Acceleration of Cometary H_2O Group Pickup Ions by Obliquely Propagating Nonlinear Magnetosonic Waves

KRISHNA M. SRIVASTAVA,• BRUCE T. TSURUTANI, AND BRUCE E. GOLDSTEIN,

Jet Propulsion Laboratory, California Institute of l'ethnology, Pasadena, California 91109

V. SHARMA* AND M. OKADA

● Defense science Research Organization, ISSA, Metcalf House, Delhi, India,

The observations made during the encounter with comet Giacobini Zinner show that the character of *MHD* turbulence is governed by the magnetosonic (*MS*) waves generated by the pickup ions via a resonant cyclotron instability. Close to the bow shock these waves are highly nonlinear, $|\Delta B/B_0| \sim 1$, and are propagating obliquely to the magnetic field. The interaction of cometary ions in the mass loaded solar wind with *MS* waves propagating away from the comet and oblique to the interplanetary magnetic field (*IMF*) is investigated using the test particle approach. Ion trajectories, distribution functions, widths of pitch angle scattering and energy diffusion are obtained. Because of the *MS* "turbulence", the particle velocity and acceleration are found to increase with increasing wave amplitude, inclination of the wave vector to the background magnetic field, and the range of resonant mode numbers. It is found that the interaction of water group pickup ions with *MS* waves propagating obliquely to the *IMF* gives larger pitch angle scattering and acceleration than that in the case of parallel and antiparallel propagating waves. In particular, obliquely propagating *MS* waves at angles greater than 40" to the ambient magnetic field are very effective at accelerating particles because of a high phase velocity along the magnetic field. In the case of monochromatic *MS* waves, Landau damping is found to play an important role; the particles get electromagnetically trapped in a potential well due to Landau damping. In the case of MS turbulence, the particles are stochastically heated and the temperature continues to grow linearly with time. We have also investigated the relationship between pitch angle scattering and the three parameters, namely , α, the angle between the solar wind flow direction and the ambient magnetic field, θ_{Bk}, the angle between the ambient magnetic field and the wave propagation vector, and the ion injection velocity. The pitch angle scattering rates are obtained using a monochromatic nonlinear *MS* wave as well as *MS* turbulence in both the quasi-parallel (0< a < 60") and quasi-perpendicular (60" c a < 90') regimes for various values of θ_{Bk}. In the case of a monochromatic *MS* wave, pitch angle scattering rates are found to change very slightly with respect to θ_{Bk}, a and the mode number of the MS wave due to their Landau damping. In the case of *MHD* turbulence the pitch angle scattering rates decrease with increasing a for $\theta_{Bk} < 40°$ and increase with increasing a for $\theta_{Bk} > 40°$. They are found to be independent of the injection velocity. The results are in agreement with the observations.

1. INTRODUCTION

The free energy available with the ring and beam distributions of cometary ions picked up by the solar wind can excite instability over a wide spectral range, We discuss here the excitation of turbulence by low frequency *MHD* waves only. The fast magnetosonic mode is the fastest growing mode among the different growing modes that can be destabilized by the ring beam distribution of the pickup ions [*Wu and Davidson,* 1972; *Thorne and Tsurutani, 1987; Brinca, 1991]* and has been observed at comets *Giacobini-Zinner* [*Smith* et al., 1986; *Tsurutani and Smith, 1986a, b]* and Halley [*Riedler et al., 1986; Neubauer* et *al.*, 1986; *Johnstone et al., 1987; Neugebauer et al., 1987, 1989, 1990; Coates et al., 1989,* 1990]. This mode has a resonant instability at the cyclotron frequency of the pickup water group ions. In both comets the high spectral power densities observed in these waves [*Tsurutani and Smith,* 1986a; *Glassmier* et *al.*, 1987] are approximately two orders of magnitude higher than the power density in the average solar wind,

Large-amplitude whistler mode wave packets were observed near comet G-Z [*Smith et al.,* 1986, *Tsurutani and Smith, 1986a,* b]. These whistler wave packets were detected at the leading edge of steepened *MS* waves [*Tsurutani et al., 1987].* It is noted that steepened magnetosonic (MS) waves are comprised of circular polarized wave fronts and linearly polarized trailing wave portions. There are also (sometimes) whistler packets leading the *MS* waves. The spectrum for the cometary waves has a power law which varies from -1.6 to -2,5,

The comet Halley waves have lower amplitudes and are more turbulent. Neugebauer et al. [1989] showed that, in the foreshock region, pitch angle scattering was much more rapid than energy diffusion for all values of a. Coates et al. [1989] showed that pitch angle scattering of cometary ions increased with reduced cometocentric distance and this diffusion rate was much greater than the energy diffusion rate. Neugebauer et al. [1990] further concluded that (1) the mean width of the proton pitch angle distribution remained relatively low and was nearly independent of cometocentric distance almost right up to the bow shock and (2) the mean width of the water group ion pitch angle distributions increased both with increasing ion density and with increasing a. The interplanetary magnetic field (*IMF*) is usually at the Parker's spiral angle relative to the solar wind (a = 45" at 1 AU), but it can exist from the quasi-parallel (O < a < 55°) to quasi-perpendicular regime (55"< a <900). The right-hand resonant instability has positive growth for a = O to 70" [*Thorne and Tsurutani, 1987; Brinca, 1991].* For angles closer to 90", the dominant instability should be the left hand resonant mode or mirror mode [*Brinca,* 1991; *Gary,* 1992]. The left hand mode was searched for under the proper conditions but was not found [*Tsurutani et al., 1989].*

Various possibilities for the heating and acceleration of plasma around comets have been proposed and discussed [*Ip and Axford,* 1986, 1990; *Tsurutani et al., 1987; Sharma et al., 1988; Yoon and* Wu, 1991, and references therein; *Galeev et al.,* 1991, and references therein]. In general four types of acceleration mechanisms have been considered: (1) second-order Fermi acceleration, (2) acceleration by diffusive shocks, namely, the first-order Fermi acceleration, (3) acceleration by magnetosonic w av es, and (4) acceleration by electrostatic hybrid waves [*Buti and Lakhina,* 1987; *Sharma and Papadopoulos, 1990].* A series of test particle calculations for the study of second order Fermi acceleration were performed *[Price and Wu,* 1987; *Luhmann* et *al.,* 1988; *Cravens,* 1986, 1989; *Terasawa, 1989; Kaya et al.,* 1989]. In this paper we have concentrated on the possibility of acceleration of pickup iona by interaction with fast nonlinear *MS* waves. In our model, the waves propagate toward the Sun obliquely to the *IMF.* We also examine particle acceleration by interaction with MH D "turbulence" which has a power spectral shape. Both studies use the test particle approach. We have also investigated the relationship between the rate of pitch angle scattering induced by wave-particle interactions via cyclotron resonance and the three parameters, namely, θ_{Bk}, the angle between the ambient magnetic field and the wave propagation vector, α, the angle the solar wind flow direction makes with the ambient magnetic field and the injection velocity v_{0b}.

The paper is organized as follows: in section 2 we discuss the model and the basic ideas. Certain physical quantities useful for comparison with observations are defined in section 3. In section 4 we present the results of the simulation and show that efficient acceleration is achieved by particles in the presence of magnetosonic turbulence. We also show the results giving the relationship between the pitch angle scattering and the three parameters, θ_{Bk}, α, and v_{0b}. In section 5, we discuss the Landau/cyclotron damping of the oblique *MS* waves and the electromagnetic trapping of particles. A summary of results of the study is given in section 6.

2. FORMULATION OF THE PROBLEM

Wave-particle interacts by parallel and antiparallel propagating MHD waves have been extensively studied and recently reviewed by Yoon and Wu [1991] and Galeev et al. [1991]. We investigate here, using the test particle method, the interaction of obliquely propagating nonlinear *MS* waves with the cometary pickup ions. The interaction occurs where these waves satisfy the cyclotron resonance condition,

$$\omega=\bar{k}\cdot\bar{v}+\Omega_i \tag{1}$$

Here ω is the frequency of the magnetosonic wave, $\bar{k}$ is the wave propagation vector, $\bar{v}$ the velocity vector of the resonant ion, and Ω_i the ion Larmor frequency of water group ion. The dispersion relation of the fast magnetosonic waves is given by [*Galeev et al.*, 1991; *Kotelnikov et al., 1991]*

$$\omega = \pm kV_A\left(1+f(\beta)k_\perp^2/k^2\right)^{1/2} \tag{2}$$

where

$$k^2=k_\parallel^2+k_\perp^2$$

and for Maxwellian solar wind protons

$$f(\beta)=\frac{-i\,\beta\sqrt{\pi}}{2}\,s\exp(-s^2)\,\phi(is) \tag{3}$$

where

$$s=\omega/\left(\sqrt{2}\,k_\parallel T_p/M_p\right)\cong\frac{1}{\beta}$$

$$\phi(x)=\frac{2}{\sqrt{\pi}}\int_0^x\exp\left(-t^2dt\right).$$

is the error function, T_p and M_p are the temperature and mass of solar wind protons and $\beta = 8\pi n_pT_p/B_0^2$ (the plasma beta), and n_p is the number density of solar wind protons, and V_A is the Alfvén speed.

It is noted from the observations that steepened MS waves are comprised of circular polarized wave fronta and linearly polarized trailing wave portions. There are also (sometimes) whistler packets leading the MS waves. From spectral analysis a variation of γ from -1.6 to -2.5 has been found. Thus we have attempted to simulate wave-particle interactions with these three "wave types" using test particle approach by following the motion of cometary ions in a given field for the three cases: (1) monochromatic, linearly polarized sinusoidal *MS* waves, (2) circularly polarized monochromatic *MS* waves, and (3) right-hand circularly polarized magnetosonic waves having a power spectrum which varies as k^{-2}. However, it may be mentioned that strictly speaking for small amplitude waves the assumption of circular polarization is not valid for obliquely propagating *MS* waves (however for large amplitude nonlinear waves of comet Giacobini-Zinner, circularly polarized obliquely propagating *MS* waves, have been claimed by *Tsurutani et al.* [1987]).

We consider the configuration of the simulation system as shown in Figure 1a. *The* background interplanetary magnetic field is represented by

$$\bar{B}_O = i\, B_O \cos \theta_{Bk} + j\, B_O \sin \theta_{Bk} \tag{4}$$

where θ_{Bk} is the angle the magnetic field makes with the wave vector and i and j are the unit vectors along x and y axes.

2.1. Linearly Polarized *MS* Waves

We have investigated the interaction of water group ions with the nonlinear monochromatic linearly polarized *MS* waves which have the form

$$B_z = A \sin (kx - \omega t + \phi_0) \tag{5}$$

The wave propagates in the x direction obliquely to the background magnetic field. Here ω is given by the dispersion relation given in (2). *A is the* amplitude of the wave and ϕ_0 is the phase of the wave. The wave number $k = k_{res}$ for *MS* waves is evaluated in the subsection 2.4. The phase, ϕ_0, is chosen randomly.

2.2. Circularly Polarized *MS* Waves

The second type of wave chosen for the study of wave-particle interactions is the right-hand circularly polarized magnetosonic wave having two components:

$$B_y = A \cos (kx - \omega t + \phi_0) \tag{6}$$

$$B_z = A \sin (kx - \omega t + \phi_0) \tag{7}$$

where k, ω, and ϕ_0 take the same values as given in the case of monochromatic linearly polarized sinusoidal *MS* waves.

2.3. Circularly Polarized Magnetosonic k^{-2} Fluctuations

The third type of calculation for wave-particle interaction was made for IUS waves having a power spectrum which varies as k^{-2} via a cyclotron resonance, A turbulent wave-field is generated by superposing circularly polarized magnetosonic waves:

$$\bar{B}_W = \sum_{k_{min}}^{k_{max}} \delta \bar{B}_k \exp (i (kx - \omega t + \phi_0)) \tag{8}$$

$$\mathrm{Re}(\bar{B}_w) = B_y \quad , \ \mathrm{Im}(\bar{B}_w) = B_z$$

propagating in thex direction obliquely to the background magnetic field given by (4). The coefficient δB_k is related to the power spectral density *P(k)* as

$$[\delta B_k]^2 = P(k)\,\Delta k \tag{9}$$

where Ak is related to the length L of the simulation box as

$$\mathrm{Ak} = 2\pi / L \tag{lo}$$

and the power spectrum $P(k)$ is assumed to vary a.. k^{-2}. We write

$$k = \quad M\,\Delta k = M\,2\pi / L \tag{11}$$

where M is the mode number of the waves in the system. The wavelength λ of the mode M is given by L/M.

The amplitude of the turbulence is given by

$$\left[\delta B\right]^2 = \sum_{k_{\min}}^{k_{\max}} \left[\delta B_k\right]^2 \tag{12}$$

Figure 1 *b* shows scattering of particles by obliquely propagating magnetosonic waves. The electric fields due to the wave and bulk motion of the plasma vanish in a frame moving along the magnetic field with velocity $V_{ph}/\cos\theta_{Bk}$, where V_{ph} is phase velocity of the waves. Scattering of particles conserves their energy in this frame. The point of injection is marked by a cross, the region of scattering is shown by the shaded shell. Note that for highly oblique ($\theta_{Bk} >$ 40") fast mode *MS* waves this velocity along the ambient magnetic field is quite large, and the particles can readily be accelerated.

2.4. Resonant Mode Numbers

The parameters for the *MS* wave and the cyclotron resonance taken are as follows: the frequency of the *MS* wave and the gyration frequency of water group ions are respectively 0.0014 Hz and 0.0425 rad s^{-1} in agreement with the observations [*Tsurutani et al.*, 1987; *Huddleston and Johnstone*, 1992]. The *MS* wave is assumed to propagate along the x-axis away from the comet. The background magnetic field makes an angle θ_{Bk} with k. In all the three cases the resonant mode numbers of *MS* waves via a cyclotron resonance are calculated from

$$M_{res} = k_{res} / \Delta k = L\ k_{res} / 2\pi \tag{13}$$

where the system size is $L = 512\ V_A / \Omega_i$ and is represented by 1024 ($=2^{10}$ an essential requirement for the fast Fourier transform to calculate the wave magnetic field) grid points. All distances are normalized by V_A / Q. Hence

$$M_{res} = \frac{512 V_A}{2\pi\Omega_l} \frac{(\omega+\Omega_l)}{v_R \cos\theta_{Bk}}$$

$$\cong 109 /(v_R^{*} \cos\theta_{Bk}),\ v_R^{*} = v_R / V_A\ , \text{ for } \frac{\omega}{\Omega_l} = 0.3 \qquad (14)$$

Here $v_R \cos\theta_{Bk}$ is the velocity of the resonant pickup ion parallel to the background magnetic field. The range of resonant mode numbers lies between 5 and 51 for v_R varying from 2VA to $22 V_A$. The power associated with large mode numbers becomes smaller and smaller as a result of the power law spectrum.

The electric field in the frame of reference moving with the average plasma velocity, neglecting Hall current and grad p_e terms which are of first order, is given by

$$\delta \bar{E} = -\bar{V}_W \times \bar{B} / c \qquad (15)$$

where $\bar{V}_W$ is the wave velocity vector and $\bar{B} = \bar{B}_O + \bar{B}_W$, $\bar{B}_O$ is the ambient magnetic field and $\bar{B}_W$ is the wave magnetic field of the turbulence generated by *MS* waves. The electrostatic field δE_x resulting from the kinetic approach using Vlasov equation has not been included in the present study.

The three-dimensional trajectories of the ions are obtained by numerically solving the equations of motion:

$$d\bar{r}/dt = \bar{v}, \qquad (16)$$

$$d\bar{v}/dt = \frac{e}{M_l}(\delta\bar{E} + \bar{v} \times \bar{B}/c) \qquad (17)$$

where $\bar{r} = \bar{i}\,x + \bar{j}\,y + \bar{k}\,z$, is the position vector, $\bar{v}$ is the velocity vector and M_i is the mass of cometary water group ion.

3. DEFINITIONS

3.1. The Power Spectrum

For the wave-particle interactions, we consider only the turbulence associated with the pickup ions. The power associated with the solar wind is 2 orders of magnitude less intense [*Tsurutani and Smith*, 1986a, b]. We assume that power spectrum in the cometary environment can be approximated as a function of wave number k [*Glassmier et al.*, 1987]

$$P(k) = A(\delta B)^2 / \left(k_0\left(1+(k/k_0)^{\gamma}\right)\right) \qquad (18)$$

where the resonant mode number for newly created pickup ions is given by $k_0 = \Omega_i / V_{sw}$, δB represents the fluctuating magnetic field, γ is the power spectral index, and the constant A is determined by the normalization $[\delta B]^2 = \int P(k)\delta k$. As $k/k_0 >>$ 1, (18) can be approximated by

$$P(k) = B\,k^{-\gamma} \qquad (19)$$

3.2. Resonant Pitch Angle Scattering

We consider pitch angle scattering of pickup ions by resonant interactions with low-frequency magnetic fluctuations generated by solar wind/cometary ion distributions. The free energy available from the pickup process causes growth of instabilities. It is well established that the instability physics changes with a. In the solar wind frame v_{0b} is the velocity of the newborn ions and a is the injection angle, This suggests that the pitch angle scattering of newborn ions from these instabilities and the resulting ion velocity distributions should be a function of a. It should be noted, however, that at comet Giacobini-Zinner onl y right hand obliquely propagating *MS* waves were detected, This is the case discussed here.

An important parameter for the comparison of model calculations and observations is the mean pitch angle width in degrees. The pitch angle θ_i of each water group ion is given by

$$\theta_i = \cos^{-1}\left(v_{\|i} / (v_x^2 + v_y^2 + v_z^2)^{1/2}\right) \qquad (20)$$

where $v_{\|i} = -v_x \cos\theta_{Bk} + v_y \sin\theta_{Bk}$. The background magnetic field makes an angle θ_{Bk} with the wave vector. The average of θ_i in the simulation is defined as

$$\left\langle \theta_i \right\rangle = \sum_{i=1}^{N} \theta_i \sin\theta_i \Big/ \sum_{i=1}^{N} \sin\theta_i \qquad (21)$$

where N is the number density of cometary ions in the box and summation extends over all the ions. Following Coates et al. [1989] and Neugebauer et al. [1990], the average width of the pitch angle distribution can be defined as

$$< \Theta > = \frac{\sum_i |\theta_i - <\theta_i>| \sin\theta_i}{\sum_i \sin\theta_i} \qquad (22)$$

This quantity is found to exhibit nontrivial temporal variations in both the quasi-parallel and quasi-perpendicular regimes and depends on θ_{Bk} and the injection angle. For an isotropic distribution, $<\Theta> =$ (n/2-1). Following *Gary et* al. [1991] we calculate the following quantity

$$< e^*(t) > \cdot \frac{\pi-2}{2} - <e(c)> \qquad (23)$$

It is instinctive to define a time-averaged pitch angle scattering (TAPAS) frequency v_ϑ through the following expression:

$$< \Theta^*(t) > = \frac{rr-2}{2} \exp(-\upsilon_\theta t) \qquad (24a)$$

which on integration yields

$$v_\vartheta / \Omega_i = (\pi/2-1) \int_0^\infty \Theta^*(t^*)\, dt^* \qquad (24b)$$

where $t^* = \Omega_i t$. We have calculated v_ϑ / Ω_i for various values of a and θ_{Bk} performing integration from t^* = O to 200.

3.3. Root Mean Square Deviation

The average velocity is defined as

$$< v > = \Sigma_i v_i / N \qquad (25)$$

and the root mean square deviation is given by

$$\sigma_v = \left\{ \frac{\Sigma_i (v_i - < v >)^2}{N} \right\}^{1/2} \qquad (26)$$

The summation is taken over all the water group ions in the systcm.

3.4. Phase Space

We define the phase space angles of the particles by the relation

$$\zeta = \tan^{-1} \frac{B_y}{B_z} - \tan^{-1} \frac{v_y}{v_z} \qquad (27)$$

where B_y, B_z, v_y, and v_z, respectively, denote the wave magnetic field and particle velocity along y and z directions. This angle is the angle by which a particle lags the wave magnetic field. For a gyrotropic distribution the particles would bc uniformly distributed. The phase space diagrams are defied as $(\zeta, v_{\|B}/V_A)$ plots and are shown in representative cases ($v_{\|B}$ is the particle velocity parallel to the ambient magnetic field).

4. RESULTS OF THE SIMULATION

The simulation geometry is shown in Figure 1*a*. The only spatial dimension is along the x axis but the velocity, magnetic and electric fields are three dimensional vectors. The solar wind flow direction makes an angle ϕ with the propagation direction which lies along the x axis. Thus the solar wind velocity is oblique to the magnetic field as is generally the case [*Neubauer et al.*, 1986; *Smith et al.*, 1986; *Tsurutani* et al., 1987]. At $t^* = \Omega_i t = O$, 1000 ions are injected which are uniformly distributed in space and have an injection velocity given by

$$v_{x0} = v_{0b} \cos\phi,\ v_{y0} = v_{0b} \sin\phi \qquad (28)$$

where $\phi = \alpha - \theta_{Bk}$.

The θ_{Bk} is varied from 20° to 80” and a is varied from 35” to 85”, The amplitude of the IUS wave was varied from 0.5 to 1.0 and that of the MS turbulence was varied from 0.25 to 0.5 ($|\Delta B/B_0|$ of the order of unity [*Tsurutani*, [1991c]). Wc present results for θ_{Bk}

equal to 60°, 40”, and 20” and *MS* wave amplitude equal to 1.0 for monochromatic *MS* wave and $|\Delta B/B_0|^2$ =0.5 for *MS* turbulence and α = 45” and show the pitch angle scattering and various distributions for each type of waves (Linearly polarized MS waves (*LPMSW*), Circularly polarized *MS* waves (*CPMS W*), and Circularly polarized magnetosonic k^{-2} fluctuations (*MST*)) for an injection velocity equal to $5V_A$ and plasma β equal to unity ($f(\beta)$= 2.0). The phase velocities of *MS* waves calculated from (2) for $f(\beta)$= 2.0, which corresponds to β equal to one are, respectively, 1.111, 1.351, and 1.58 times the Alfvén velocity for θ_{Bk} equal to 20”, 40”, and 60”. The phase velocities for $f(\beta)$ = 1.8,, which corresponds to β - 0.9 are, respectively, $1.204V_A$, $1.434V_A$, $1.574V_A$, and $1.657V_A$ for θ_{Bk} equal to 30°,50”,65 “, and 80”.

All the Figures 2 to 5 and 8 to 10 labelled *a*, *b*, c, *d*, and e show, respectively, the ion distribution function ($v_{\|B}/V_A$, $v_{\perp B}/V_A$), *the* phase space diagrams, (ζ, $v_{\|B}/V_A$), the width of the energy diffusion (v/V_A, $v^2 f$), *the* width of pitch angle scattering $\left\langle \theta^{*}(t) \right\rangle$, and evolution of ion velocity distribution (σ_v/V_A, < v > $/V_A$) or ($\Omega_i t$,< v > $/V_A$). The $v_{\|B}$, $v_{\perp B}$ and f are the velocities parallel and perpendicular to the ambient magnetic field and the phase space density of ions. The quantities < v > and σ_v denote the average velocity of particles and root mean square deviation, and ζ has been defined by (27). We have obtained results for various angles θ_{Bk}, a and amplitudes. We show results for θ_{Bk} = 20”, 40°, 60”, a = 45°, and A = 1.0 for monochromatic *MS* wave and $|\Delta B/B_0|^2$ =0.5 and 0.2S for IUS turbulence.

We have also investigated the relationship between the pitch angle scattering, θ_{Bk} , a, and v_{0b} for the cases of *CPMSW* and *MST*. Figures. 6 and 12 show (σ_v/V_A, < v > $/VA$) relation for *CPMSW* and *MHD* turbulent spectrum for various θ_{Bk} and a = 55”. The pitch angle scattering rates are shown for *CPMSW* in Figure 7 and for *MS* turbulence in Figure 11.

Case 1: Linearly polarized *MS* waves (*LPMSW*). Test particle calculations are performed for resonant mode number, M_{res} = 18, $f(\beta)$ = 2.0 (β= 1.0), a = 45° and injection velocity equal to *5VA* for various angles θ_{Bk}, and wave amplitudes. The results are shown at time t^*=200 for a wave amplitude, A = 1.0, and one angle, namely, θ_{Bk}=60° in Figures 2a, 2b, *2c*, and 2d. We have chosen the same values in each case for making comparison in the three cases. From Figures *2a* and *2c*, it can be seen that efficient acceleration and energy diffusion due to a monochromatic *LPMSW* propagating unidirectionally away from the comet, can be achieved depending on the angle, θ_{Bk} and the amplitude of the wave of she order of unity. Large-amplitude magnetosonic waves have been observed near comets (r<2x10^5 *Tsurutani, [1991]*). The pitch angle scattering *(PAS)* is found to be more efficient than the energy diffusion. The widths of the ion distribution functions in phase space and energy increase with the wave amplitude and increasing θ_B k. The time-averaged pitch angle scattering *(TA PA S)* frequencies for θ_{Bk}=20° and 60” are, respectively, 0.66 Ω_i and

0.61 Ω_i. The evolution of the ion velocity distribution functions ($\Omega_i t$, < v > /VA) shown in Figure *2d* indicates that the average velocity of **particles oscillates** about < v > = $5.4V_A$, $7.7 V_A$, and $9.1 V_A$ for θ_{Bk} =20°, 40° and 60° depending on the wave amplitude and the angle between the wave vector and the background magnetic field. The average velocity <v> about which particles oscillate naturally increases with the increase in the wave amplitude and increase in θ_{Bk}. The Landau damping plays an important role in the case of *CPMS W: the MS* waves are damped and the particles get electromagnetically trapped and oscillate in a moving magnetic mirror and further heating of ions, further wave damping does not take place.

Case 2: Right-hand circularly polarized *MS* waves (*CPMSW*). Results of the simulation are shown in Figures *3a* to *3d* , 4, *5a,* and 5 *b* for the mode number, M_{res} = 18 for an injection velocity equal to $5V_A$ for θ_{Bk} = 60° ,40", 20° , *a*= 45° for wave amplitude, *A* = 1.0. The evolution of the distribution function ($v_{\|B}/V_A$, $v_{\perp B}/V_A$), *the* phase space diagram (ζ, $V_{\|B}/V_A$) and (v/V_A , v2f) at fixed time $t^* = \Omega_i\ t$ = 200 are shown in Figures 3 to 5 labeled *a, b,* and c respectively. It is evident from all the figures shown that efficient acceleration is achieved even for moderate amplitudes of monochromatic MS waves propagating unidirectionally and obliquely to the ambient magnetic field for θ_{Bk} > 40° (say *A*=0.5). *PAS is* found to be more rapid than energy diffusion for these cases. The *PAS* and the width of the energy diffusion ($v^2 f$) are found to increase with both the wave amplitude and θ_{Bk} . It is seen from the figures labeled *d* that the width of the pitch **angle** scattering, < $\Theta^*(t\ )$ > = $(\pi\ -2)/2$ -< $\Theta(t\ )$ > , decreases with time. The **evolution** of the ion velocity distribution ($\Omega_i t$, < v > /V_A) is shown in Figure *5b* for θ_{Bk} = 60", 40", 20", and amplitude equal to 1.0. It can be seen from Figure *5b* that particles, after achieving a maximum velocity at a certain time depending on the wave amplitude and the **angle** between the wave vector and the background magnetic **field** start decelerating, achieve a minimum velocity and accelerate again. The average velocity of particles oscillates about c v > = $5.08V_A$, $7.3V_A$, and $13.1V_A$ for θ_{Bk} = 20", 40", and 60" respectively. Particles in the presence of large amplitude waves with high compression get accelerated faster. The Landau damping plays an important role in the case of monochromatic circularly polarized *MS* waves also: the *MS* waves get damped and particles are electromagnetically trapped by the waves and oscillate in a moving magnetic mirror and further heating of ions **does** not take **place.**

Test particle calculations are also performed to study the relationship between the *PAS,* θ_{Bk}, α, and v_{0b} for resonant mode number, M_{res} = 18 for various wave amplitudes for an injection velocity given by (28). The *TAPAS* frequency, average velocity, rms deviation , and width of *PAS are* obtained at t^* .200 with Δt^* = 0.05 for wave amplitude *A* = 0.5 and θ_{Bk} = 50° , 65", and 80° and a = 35", 55', and 85". The evolution of the ion velocity distribution (σ_v/V_A ,< *v* > */VA) is* shown in Figure 6 for θ_{Bk} = 50', 65', and 80" and a = 55" which shows that the average velocity of particles oscillates in a certain range depending on the wave amplitude and the angle between the wave vector and the background magnetic field. σ_v and < v > are the root mean square deviation and the average velocity. This again confirms that the particles get electromagnetically trapped in a potential well due to Cherenkov resonance. The Landau/cyclotron damping of *MS* waves is discussed in section 6, The *TAPAS* frequency is shown against α for various θ_{Bk} in Figure 7. It can be seen from Figure 7 that for θ_{Bk} = 30° and 50° the *TAPAS* frequency changes slightly asa increases from 35° to 85°, whereas for θ_{Bk} = 65° and 80°, the *TAPAS* frequency increases as *a* increases from 35' to 55" and then again decreases at α=85°. This is due to the explicit dependence of *PAS* through (20) and its implicit dependence on the direction of injection of ions, *a*. It is found that v_ϑ / Ω_i depends on the resonant mode number of the waves, θ_{Bk} and a.

Case 3: Magnetosonic turbulent fluctuations (*MST*). We have studied the interaction of cometary pickup ions with magnetic fluctuations generated by circularly polarized *MS* waves via cyclotron resonance for β=1.0 ($f(\beta)$ = 2.0) and *a* = 45". Results arc obtained for various angles and wave amplitudes and are shown in Figures 8a to 8*d*, 9, 10a, and 10b for angles θ_{Bk} = 60",40", and 20" at time t^* = 200 and level of turbulence, $|\Delta B/B_0|^2$ equal to 0.5 (lM/Bol = 0.7 in agreement with the observations [*Tsurutani*, 199 1a] for a range of mode numbers from 5 to 51. It cars be seen from the Figures labelled *a* and c that the pitch angle scattering is faster than the energy diffusion for these cases . As θ_{Bk} moves from the quasi-parallel (0° c θ_{Bk} <40") to quasi-perpendicular regime (40° < θ_{Bk} < 80'), particle acceleration increases appreciably due to the increase in the phase velocity of the *MS* waves. The average width of the pitch angle scattering is found to decrease as time increases. *MHD* turbulence enhances pitch angle scattering greatly and is found to be much more than that for *CPMSW* in which case it is reduced by Landau damping. It is found that the Landau damping of IUS waves is less effective in the case of *MHD* turbulence due to stochastic effects, The ion velocity distribution function for θ_{Bk} = 60',40', and 20' shown in Figure 10b show almost no oscillatory behavior as the particles get highly accelerated due to the interaction with *MHD* turbulence.

PAS width, *TAPAS* frequency and width of energy diffusion (v^2f) are also obtained for turbulence levels, $A = (|\Delta B/B_0|)^2$ = 0.5 and 0.25, for various angles θ_{Bk} = 30' to 80" and a = 35", 55", and 85" and for mode numbers lying between 5 and 51 at time t^* = 200. The results are shown in Figures 11 and 12 for one representative case only. The v_ϑ/Ω_i is shown against *a* in Figure 11 for θ_{Bk} = 30', 50°, 65", 80", and *A=O.25.* It is found that pitch angle scattering rate decreases for θ_{Bk} <40' with increasing a, while it increases with increasing a for θ_{Bk} > 40°; i.e., the *TAPAS* frequency decreases with *a in the* quasi-parallel regime (O" < θ_{Bk} < 40°), while it increases with *a in* the quasi-perpendicular regime (40" < θ_{Bk} < 80"). This is because more pitch angle scattering takes place in the quasi-perpendicular regime than in the quasi-parallel regime. The evolution of ion velocity distribution, (σ_v/V_A , < *v* > /V_A) for θ_{Bk} = 50", 65", and 80" for wave amplitude equal to 0.5 is shown in "Figure 12.

Table 1 provides a summary of results, namely, v_ϕ/Ω_i (time-averaged rate of scattering frequency normalized to water group ion cyclotron frequency), minimum and maximum values of $v_{\|B}/V_A$, $v_{\perp B}/V_A$ (velocities parallel and perpendicular to the ambient magnetic field), σ_v/V_A, mot mean square deviation, $<v>$ (average velocity), and the maximum of the width of energy diffusion ($v^2 f/2000$), for θ_{Bk} = 20”, 4(Y, and 60° and a = 45” for all the three cases.

5. THE LANDAU DAMPING OF MAGNETOSONIC WAVES

The physical processes underlying Landau and cyclotron damping are quite similar. In each case a beam traveling in the neighborhood of a critical velocity gives to or absorbs energy” from the electromagnetic field, depending on whether the beam drift velocity is slightly greater or smaller than the phase velocity of the wave. The exchange of energy between particles and the wave field causes periodic oscillations in the parallel and perpendicular velocities. Such periodic motions are analogous to the oscillations of charged particles in an electromagnetic potential well. In the comet-solar-wind interaction regions with comets the value of plasma β is of the order of unity or even larger (for Halley it is larger than unity) and the phase velocity of the oblique *MS* waves is comparable with the thermal velocity of protons, According to the quasi-linear theory [Kotelnikov et al., 1991], the oblique *MS* waves produce a plateau on the thermal protons distribution because of Cherenkov resonance. The Cherenkov resonance in a finite β plasma causes strong damping of oblique *MS* waves.

The darnping of oblique *MS* waves maybe caused by (1) Landau damping due to Cherenkov resonance as described above, and (2) the cyclotron damping due to wave-particle resonance in the presence of magnetic field. The conditon for electromagnetic trapping of particles is given by

$$\omega - k_{\|} v_{\|} \pm n\Omega_i = 0 \tag{29}$$

where n is an integer. Landau (Cherenkov) resonance occurs for n=0 and cyclotron resonance for n=1, 2, 3, ..,. The simulation results show that oblique monochromatic *MS* waves propagating at angles θ_{Bk} >40’ impart efficient acceleration to particles whereas those propagating at angles θ_{Bk} <40” show weak wave-particle interactions due to their phase velocity being very close to the Alfvén velocity. The damping of *MS* waves is caused by Cherenkov resonance. The effect of damping at large times is very much suppressed in the case of *sUHD* turbulence. The square of the maximum and minimum magnetic field for the two cases, namely, *CPMSW* and *LPMSW are*, respectively, given by 1 + 2A $\sin\theta_{Bk} + A^2$, 1- 2A $\sin\theta_{Bk} + A^2$ and 1 + A^2, *1.* The trapping is more prominent in the case of *CPMSW as* compared to *LPMSW* because (1) the mirror ratio for the former is larger, and (2) the larger wave magnetic field causes larger pitch angle for the former.

The quasi-linear them-y is valid for finite but small-amplitude waves only. The simulation has been performed for large-amplitude waves ($A \sim 0.4$) which show strong wave-particle interactions.

Table 2 shows the Landau darnping mechanism (value of n) for different angles of propagation, the magnetic mirror ratio, R ($R = B_{max}/B_{min}$), the probability for the trap ($p = \int \cos\theta d\theta$, from θ = O to $\theta = \theta_0$ where θ is the pitch angle and $\theta_0 = \sin^{-1}(B_{min}/B_{max})$), the maximum and minimum of $(\omega - k_{\|}v_{\|})/k$. It can be seen that $(\omega - k_{\|}v_{\|})/k$ goes to zero for $\theta_{Bk} = 20°$ to 60". Thus the particles get electromagnetically trapped in a potential well due to Cherenkov resonance. The Landau damping of MS waves and the electromagnetic trapping of ions can be seen from the Figures 2d, and 5b showing ($\Omega_i t$, < v >/VA) for *LPMSW* and *CPMS W.*

6. SUMMARY AND CONCLUSIONS

We have performed the test particle calculations to study wave particle interactions via cyclotron resonance of water group cometary ions with (1) linearly polarized monochromatic *MS* waves, *(2)* circularly polarized monochromatic *MS* waves, and (3) magnetic fluctuations consisting of *MS* waves with a power spectrum which varies as $1/k^2$. We have made the quantitative comparisons between the results in the three cases for *MS* waves propagating toward the Sun. Different types of Alfvenic fluctuations are naturally associated with different degrees of isotropization of the ion distributions. Tsurutani et al. [1987, 1989], noted that very far from the comet *G-Z* (7×10^5 km) waves were predominantly elliptically polarized, long-wavelength MHD waves. At intermediate distances ($\approx 3\times10^5$ km), the waves were more compressive. The steepened MS waves had partial (circularly polarized) rotation, linearly polarized portions and were sometimes preceded by high-frequency wave packets. Near the comet ($r <$ 2x105 km) the fluctuations had large-amplitudes ($|\Delta B/B_0| \approx 1$), were highly compress ional, and had a turbulentlike power spectrum. These observations suggest that for $r > 3\times10^5$ km, the calculations with monochromatic waves are more appropriate, whereas closer to the comet, calculations with *MS* turbulence are more appropriate. Cravens [1989] calculations did not include Fermi acceleration because the magnetic fluctuations did not propagate *(VA =0).* Test particle calculations of Terasawa [1989] were done for parallel and antiparallel propagating Alfvenic fluctuations which had no compressive components. Our calculations of interaction of pickup ions with magnetosonic waves propagating obliquely to the *IMF* indicate larger pitch angle scattering and acceleration than in the case of parallel and anti-parallel propagating Alfvén waves [*Terasawa, 1989 ; Gary et al.,* 199 1] This is mainly due to the following reasons: (1) the amplitude of the *MS* waves is much larger and are compressive in this study and (2) the component of the velocity of the wave (scattering center) parallel to the magnetic field for obliquely propagating *MS* waves is larger than the Alfvén velocity.

The main inclusions of the study are summarized below:

1. It is found that efficient pitch angle scattering and energy diffusion takes place in all the three cases for θ_{Bk} >30". The order of magnitude for *PAS is* found as

$$(PAS)_{LPMSW} < (PAS)_{CPMSW} < (PAS)_{MST}$$

This is physically reasonable because the wave magnetic field follows the same ordering. In addition particle acceleration markedly increases as the direction of propagation moves from the quasi-parallel to quasi-perpendicular regime due to the increase in the phase velocity of *MS* waves. *PAS* also increases with increasing compression.

2. The particle velocity and acceleration arc found to increase with increasing θ_{Bk}, the amplitude of IUS waves and the range of resonant mode numbers. It is also found that, in the cases of ***LPMSW*** and ***CPMSW***, particle velocity and acceleration oscillate in a certain range depending upon the wave amplitude and the angle between the wave vector and the background magnetic field (as can be seen from the evolution of ion distributions shown in Figure *5b*. Ions, after gaining a maximum in velocity and acceleration start decelerating, reach a minimum in velocity and acceleration, and then accelerate again. This cyclical process continues forever (in the simulation). This feature is due to the magnetosonic waves being Landau damped and the particles being trapped by the electromagnetic field of the wave. The Cherenkov/cyclotron resonance mechanism is found to be active. The effect of electromagnetic trap is somewhat reduced for large-amplitude waves with large compression. However, the oscillations with lesser amplitude persist due to the effect of damping. The effect of Landau damping of magnetosonic waves as found in the simul at ions can be ordered as follows:

(Landau damping) ***CPMSW*** > (Landau damping) ***LPMSW***

The trapping is more prominent in the case of ***CPMSW*** as compared to ***LPMSW*** because of (1) the larger probability for the trap in the case of the former, and (2) the larger wave magnetic field which causes larger pitch angle for the former.

3. In the cases of interactions with *LPMSW* and ***CPMSW***, *the* H_2O group ion time averaged pitch angle scattering frequency with respect to a follows a somewhat different pattern from the ***MS*** turbulence. It changes slightly as a increases from 35’ to 85”, whereas for θ_{Bk} = 65” and 80’, the *TAPAS* frequency increases as a increases from 35” to 55” and then again decreases at $\alpha=85^\circ$. This is due to the explicit dependence of *PAS* through (20) and its implicit dependence on the direction of injection of ions, a. In the case of *MHD* turbulence, they increase as a increases, for $\theta_{Bk} > 40^\circ$ whereas they decrease with increasing α for $\theta_{Bk} < 40^\circ$.

4. In the case of a monochromatic *MS* wave, pitch angle scattering rate is found to change very slightly with respect to θ_{Bk}, a and the mode number of the MS wave due to their Landau damping. It is found to be independent of the injection velocity also.

5. The width of energy diffusion (v^2f), the average velocity and root mean square deviation, increase as the angle of wave propagation moves from the quasi-parallel to quasi-perpendicular regime. The increase is higher by a factor of approximately 2 for $\theta_{Bk}=80^\circ$ than for $\theta_{Bk}=30^\circ$. They also increase as a increases from 35” to 85” in both the cases.

6. It is evident from the study that the angle of injection (solar wind flow direction) and the direction of propagation of waves play an important role in governing the mechanism of wave-particle interaction via cyclotron resonance. This is in agreement with the studies of Brinca [1991] and Gary et al. [1991] and with the observations [*Neugebauer et al.*, 1990].

7. Table 1 provides information about maximum and minimum in the respective physical quantities achieved by particles for $\alpha = 45°$. Velocity and acceleration of a particle parallel and perpendicular to the ambient magnetic field, root mean square deviation and average velocity of particles increase as θ_{Bk} changes from 20" to 60". Pitch angle scattering width $(\langle\Theta(t)\rangle_{max} - \langle\Theta(t)\rangle_{min})$ is proportional to v_{ϑ} / Ω_i (*TAPAS*). The $v^2 f$ values provide a measure of energy diffusion in arbitrary units.

As suggested by Ye et al. [1993] we also obtained results assuming a wave spectrum varying as $k^{-2.5}$ and found that they were similar to those for an assumption of k^{-2} spectrum with a difference of only approximately 2 % in all the physical quantities.

Although only unidirectional IUS waves propagating away from the comet have been considered here, it would be worthwhile to investigate wave particle interactions via cyclotron resonance by adding anti-sunward propagating IUS waves (assuming that 5-10% of the total wave energy propagates toward the comet). Coates et al. [1992] have observed antisunward propagating waves at comet Halley. The input from the observations for the *IMF* and randomly distributed particles with probability proportional to gas production rate instead of uniformly distributed in space will have significant effect on the overall wave particle interactions due to magnetosonic turbulence. Research on this challenging topic is in progress.

Acknowledgments. This work was done at the Jet Propulsion Laboratory, California Institute of Technology under contract with the National Aeronautics and Space Administration. This work was performed during the period Krishna M, Srivastava held a Senior Resident Research Associateship administered by the National Aeronautics and Space Administration through the National Research Council. Useful discussions with M. Neugebauer, Y. Omura, and N. Omidi are thankfully acknowledged. We thank the referees for useful comments which improved the paper greatly.

The Editor thanks K. Kecskeme'ty and another referee for their assistance in evaluating this paper.

REFERENCES

Brinca, A. L., Cometary linear instabilities: from profusion to perspective, in *Cometary Plasma Processes, Geophys. Monogr. Ser., vol.* 61, edited by A. D. Johnstone, p. 211, AGU, Washington, D. C., 1991.

Brinca, A. L., and B. T. Tsurutani, On the polarization, compression and non-oscillatory behaviour of hydromagnetic waves associated with pickup ions, *Geophys. Res. Lett.*, 14,495, 1987.

Brinca, A. L., and B. T. Tsurutani, Survey of low frequency electromagnetic waves stimulated by two coexisting newborn ion species, *J. Geophys. Res.*, 93,48, 1988.

Brinca, A. L., and B. T. Tsurutani, The oblique behaviour of low frequency electromagnetic waves excited by newborn cometary ions, *J. Geophys. Res.*, *94*, 3, 1989.

Buti, Et., and G. S. Lakhina, Stochastic acceleration of cometary ions by lower hybrid waves, *Geophys. Res. Lett.*, 14, 107, 1987.

Coates, A. J., A. D. Johnstone, D. E. Huddleston, B. Wilken, K. Jockers, and K. -H. Glassmeier, Velocity space diffusion of pickup ions from the water group at Comet Halley, *J. Geophys. Res., 94,* 9983, 1989, (Correction, 95,4343, 1990).

Cravens, T. E., Ion distribution functions in the vicinity of comet Giacobini-Zinner, *Geophys. Res. Lett.*, 13,275, 1986.

Cravens, T. E., Test parrticle calculations of pickup ions in the vicinity of comet Giacobini-Zinner, *Planet. Space Sci., 37, 1169,* 1989.

Galeev, A. A., R. Z. Sagdeev, V. D. Shapiro, V.I. Schevchenko, and K. Szego, Quasilinear theory of the ion cyclotron instability and its application to the cometary plasma, in *Cometary Plasma Processes, Geophys. Monogr. Ser.*, vol. 61, edited by A, D. Johnstone, p 223, AGU, Washington D. C., 1991.

Gary, S. P. , The mirror and ion cyclotron aniisotropy instabilities, *J. Geophys. Res.*, 97, 8519, 1992.

Gary, S. P., R. H. Miller, and D. Winske, Pitch angle scattering of cometary ions: Computer simulation, *Geophys. Res. Lett., 18, 1067,* 1991.

Glassmier, K.-H., F. M. Neubauer, M. H. Acuna, and F. Mariani, Low frequency magnetic field fluctuations in comet P/Halley's magnetosheath: Giotto observations, *Astron. Astrophy., 187, 65, 1987.*

Huddleston, D. E., and A. D. Johnstone, Relationship between wave energy and free energy from pickup ions in the comet Halley environment, *J. Geophys. Res.*, 97, 12,217, 1992.

Ip, W.-H., and W. I. Axford, The acceleration of particles in the vicinity of comets, *Planet. Space Sci.*, 34, 1061, 1986.

Ip, W.-H., and W. I. Axford, The Plasma, in *Physics and Chemistry of Comets eedited* by W. F. Heubner, (p. 177, Spring er-Verlag New York, 1990).

Johnstone, A. D., et al., Alfvenic turbulence in the solar wind flow during the approach to comet P/Halley, *Astron. Astrophys., 187, 25, 1987.*

Kaya, N., H. Matsumoto, and B. T. Tsurutani, Test particle simulation study of whistler wave-packets observed near comet Giacobini-Zinner, *Geophys. Res. Lett.,* 16,25,1989.

Kotelnikov, A. D., M. A. Polyudov, M, A. Malkov, R. Z. Sagdeev, and V. D. Shapiro, High amplitude magnetosonic waves in the upstream region of the cometary bow shock, *A stron. Astrophys., 243,546,* 1991.

Luhmann, J. G., J. A. Fedder, and D. Winske, A test pick-up model of pick-up ions at comet Halley, *J. Geophys. Res.*, 93,7352, 1988.

Miller, R. H., S. P. Gary, D. Winske, and T. I. Gombosi, Pitch angle scattering of cometary ions into monospherical and bispherical distributions, *Geophys. Res. Lett.*, 18, 1063,1991.

Neubauer, F. M. , et al., First results from the Giotto magnetometer experiment at comet Halley, Nature, 321, 352, 1986.

Neugebauer, M., et al., The variation of protons, alpha particles, and the magnetic field across the bow shock of comet Halley, *Geophys. Res. Lett.,* 14, 995, 1987.

Neugebauer, M. , A. J. Lazarus, H. Balsiger, S. A. Fuselier, F. M. Neubauer, and H. Rosenbauer, The velocity distribution of cometary protons picked up by the solar wind, *J. Geophys. Res., 94,5227,* 1989.

Neugebauer, M., A. J. Coates, and F. M. Neubauer, Comparison of picked-up protons and water group ions upstream of comet Halley's bow shock, *J.. Geophys. Res.*, 95, 18,745, 1990.

Price, C. P., and C. S. Wu, The influence of strong hydromagnetic turbulence on newborn cometary ions, *Geophys. Res. Lett., 14, 856, 1987.*

Reidler, W., K. Schwingenschuh, Ye. G. Yeroschenko, V. A. Styashin, and C. T. Russel, Magnetic field observations in comet Halley's coma, Nature, 321, 288, 1986.

Sagdeev, R. Z., V. D. Shapiro, V. I. Schevchenko, and K. Szego, MHD turbulence in the solar wind-comet interaction region, *Geophys. Res. Lett.*, 13, 85, 1986.

Sharma, A. S., and K. Papadopoulos, Ion-ion hybrid resonance heating at comet-solar wind interaction, *Bull. Am. Phys. Soc., 35, 2098, 1990,*

Sharma, A. S., P. J. Cargill, and K. Papadopoulos, Resonance absorption of Alfven waves at the comet-solar wind interaction regions, *Geophys. Res. Lett.*, 15, 740, 1988,

Smith, E. J., B. T. Tsurutani, J. A. Slavin, D. E. Jones, G. L. Siscoe, and D. A. Mendis, International Cometary Explorer encounter with Giacobini-Zinner: Magnetic field observations, Science, 232,382, 1986.

Stix, T. H., *The* Theory *of Plasma waves*, McGraw-Hill, New York, 1962.

Terasawa, T., T. Mukai, W. Miyake, M. Kitayama, and K. Hirao, Detection of cometary pickup ion up to 10 km from comet Halley: Suisei observations, *Geophys. Res. Lett.*, 13,837, 1986.

Terasawa, T. Particle scattering and acceleration in a turbulent plasma around comets, in *Plasma Waves and Instabilities at Comets and in Magnetospheres, Geophys. Monogr. Ser., vol. 53,* edited by B. T. Tsurutani and H. Oya, p. 41, AGU, Washington D. C., 1989.

Thorne, R. M., and B. T. Tsurutani, Resonant interactions between cometary ions and low frequency electromagnetic waves, *Planet. Space Sci.*, 35, 1501, 1987.

Tsurutani, B. T., Comets: A laboratory for plasma waves and instabilities, in *Cometary Plasma Processes, Geophys. Monogr. Ser.*, vol. 61, edited by A. D. Johnstone, p. 189, AGU, Washington, D. C., 1991a.

Tsurutani, B. T., Nonlinear low frequency (LF) waves: Comets and foreshock phenomena, in *Physics of Space Plasmas,* edited by T. Chang, G. B. Crew and J. R. Jasperse, p. 91, AGU, Washington D. C. ,1991b.

Tsurutani, B. T., Cometary plasma waves and instabilities, in Comets in the Post Halley Era, vol. 2, edited by R. L. Newburn, Jr. et al., p. 1171, 1991c.

Tsurutani, B. T., and E. J. Smith, Strong hydromagnetic turbulence associated with comet Giacobini-Zinner, *Geophys. Res. Lett., 1*3, 259, 1986a.

Tsurutani, B. T. and E. J. Smith, Hydromagnetic waves and Instabilities associated with cometary ion pickup: ICE observations, *Geophys. Res. Lett.*, 13, 263, 1986*b*.

Tsurutani, B. T., R. M. Theme, E. J. Smith, J. T. Gosling, and H. Matsumoto, Steepened magnetosonic waves at comet Giacobini-Zinner, *J. Geophys. Res.*, 92,11,074, 1987.

Tsurutani, B. T., E. J. Smith, A. L. Brinca, R. M. Theme and H. Matsumoto, Properties of whistler mode wave packets at the leading edge of steepened magnetosonic waves: Comet Giacobini - Zinner, *Planet. Space Sci.*, 37,167, 1989.

Wallis, M. I., and R. S. B. Ong, Strongly cooled ionizing plasma flows with applications to beams, *Planet. Space Sci.*, 23, 713, 1975.

Wu, C. S., and R. C. Davidson, Electromagnetic instabilities produced by neutral-particle ionization in interplanetary space, *J. Geophys. Res.*, 77,5399, 1972.

Ye, G., T. E. Cravens, and T. I. Gombosi, Pickup protons and water ions at comet Halley: Comparison with Giotto observations, *J. Geophys. Res.*, 98, 1311, 1993.

Yoon, P. H. and C, S. Wu, Ion pickup in the solar wind via wave-particle interactions, in *Cometary Plasma Processes, Geophys. Monogr. Ser., vol.* 61, edited by A. D. Johns[one, p. 241, AGU,Wa..hington, D. C., 1991 .

TABLE 1. Maximum and Minimum Values of Physical Quantities in the Simulation

	LPMS W $M = 18$ $A = 1.0$		*CPMS W* $M = 18$ $A = 1.0$		*MIID* TURBULENCE $M = 5\text{-}51, \underline{A} = 0.5$	
	Minimum	Maximum	Minimum	Maximum	Mimimum	Maximum
θ_{Bk} = 20° V_ϑ/Ω_i		= 0.662	0.41		0.79	
$v_{\|B}/V_A$	-6.75	4.11	-6.80	2.72	-12.10	10.0
VAB $/V_A$	0.03	5,95	0.055	5.61	0.07	13.9
σ_v/V_A	0.15	1.48	0.063	1.39	0.23	2.14
$<v>/V_A$	3.99	5.07	3.66	5.1	4.82	7.24
$v^2f/2000$	0.993		1.26		1.444	
θ_{Bk} = 40° V_ϑ/Ω_i		= 0.565	0.41 ‘1	0.787		
$v_{\|B}/V_A$	-10.360	5.10	-10.18	4.32	-22.50	17.54
$v_{\wedge B}/V_A$	0.031	8.95	0,215	8.48	0.24	21.55
σ_v/V_A	0.200	2.86	0.16	2.54	0.29	4.34
$<v>/V_A$	5.110	6.38	4.85	7.36	5.16	12.27
$v^2f/2000$	1.26		2.44		3.03	
θ_{Bk} = 60° V_ϑ/Ω_i		= 0.61	0.43	0.74		
$v_{\|B}/V_A$	-16.05	6.34	-17.17	5.20	-31.49	23.67
$v_{\wedge B}/V_A$	0.18	12.88	0.05	12.11	0.60	35.16
σ_v/V_A	0.21	4.04	0.28	5.50	0.476	6.43
$<v>/V_A$	5.46	9.21	5.24	13.23	5.40	17.62
$v^2f/2000$	1.85		2.90		4.84	

All values are at t* =200, $f(\beta)=2.0$ ($\beta=1$ .0), and A =1 .0. This table provides she information regarding the maximum and minimum of velocities parallel and perpendicular to the background magnetic field, root mean square deviation, average velocity and the maximum of the width of energy diffusion ($v^2f/2000$) for θBk=20° , 40”, and 60”, and a =45°

TABLE 2. Landau Damping Mechanism

θ_{Bk}	n	R	P	$(\omega - k_{\parallel} v_{//})/k$ Maximum	Minimum
CPMSW: M =18, A =1, β = 0.9, α =45°					
20°	o	1.76	0.57	0.547	-2.56
40'	0	4.60	0.88	0.087	-2.89
60°	0	13.8	0.96	0.7	-4.2
LPMSW: *M* =18, *A* =1, β = 0,9, *a* =45°					
20"	o	1.42	0.54	0.007	-2.57
40"	0	1.42	0.54	0.085	-2.37
40"	0	1.42	0.54	0.754	-1.9
CPMSW: *a* =85⁴, *A* =0.4, β=1, *M* =18					
30'	o	1.53	0.76	1.06	-2.90
50°	0	2.04	0.90	1.52	-0.82
65"	0	2.50	0.92	0.83	-0.65

All values are at t* =200, $f(\beta)$=2.0 (β =1 .0).

FIGURE CAPT'1ONS

Fig. 1*a*. Schematic diagram of the simulation geometry. The wave propagates along x axis.

Fig. 1*b*. Scattering of particles by obliquely propagating magnetosonic waves. The electric fields due to the wave and bulk motion of the plasma vanish in a frame moving along the magnetic field with velocity $-V_{ph}/\cos(\theta_{Bk})$, where V_{ph} is phase velocity of the wave. Scattering of particles conserves their energy in this frame. The point of injection is marked by a cross, and the region of scattering is shown by the shaded shell.

Fig. 2*a*. The velocity distribution of ions observed at $\Omega_i t$ = 200 for linearly polarized IUS waves of amplitude, A = 1.0, M_{res} = 18, and θ_{Bk} = 60", α = 45" for plasma β = 1.0. The velocities are parallel and perpendicular to the ambient magnetic field.

Fig. 2*b*. The phase space diagram $(\zeta, v_{||B})$ of ions for the same parameters as for Figure 2a.

Fig. 2*c*. Energy distribution $(v^2 f/2000)$ in arbitrary unit against *v/VA for the same* parameters as for Figure 2*a*.

Fig. *2d. The* average velocity, < v > / *VA* of ions as a function of time t^* for the same parameters as for Figure 2a. The three curves refer to θ_{Bk} = 20",40', and 60°.

Fig. 3a. The velocity of ions observed at Slit= 200 for circularly polarized *MS* waves of amplitude, *A* = 1.0 and θ_{Bk} =60" , a = 45" for plasma β = 1.0. The velocities are parallel and perpendicular to the ambient magnetic field.

Fig. *36. The* phase space diagram $(\zeta, v_{||B})$ of ions for the same parameters as for Figure 3*a*.

Fig. 3c. Energy distribution $(v^2 f/2000)$ in arbitrary unit against *v/VA* for the same parameters as for Figure 3*a*.

Fig. *3d* . The width of pitch angle scattering $<\Theta^*(t)> = (\pi-2)/2 - <\Theta(t)>$ against time for the same parameters as for Figure 3a.

Fig. 4. The velocity distribution of ions observed at $\Omega_i t$ = 200 for circularly polarized *MS* waves of amplitude, *A* = 1.0 and θ_{Bk} =40°, a = 45" for plasma β = 1.0. The velocities are parallel and perpendicular to the ambient magnetic field.

Fig. 5*a*. The velocity distribution of ions observed at $\Omega_i t$ = *200* for circularly polarized *MS* waves of amplitude, *A = 1.0* and θ_{Bk} = 20°, a = 45' for plasma β = 1.0. The velocities are parallel and perpendicular to the ambient magnetic field.

Fig. 5*b*. The average velocity of ions against root mean square deviation for the same parameters as for Figure 5a. The three curves refer to θ_{Bk} = 20", 40°, and 60'.

Fig. 6. The average velocity, < v >/VA against root mean square deviation, σ_v/V_A for circularly polarized *MS* waves of amplitude, *A* = 0.5 and θ_{Bk} = 50',65', 80° , a= 55'.

Fig. 7. The time averaged pitch angle scattering frequency as a function of injection rate observed at $\Omega_i t$ = 200 for circularly polarized MS wave of amplitude, A = 0.5 and θ_{Bk} = 30°, 50',65', and 80" for plasma b of O(1) and a = 35", 55", and 85".

Fig. *8a. The* velocity distribution of ions observed at $\Omega_i t$ = 200 for MHD turbulence generated by circularly polarized MS waves of amplitude, $|\Delta B/B_0|^2 = 0.5$ and θ_{Bk} =60”, a = 45’ for plasma β= 1.0. The velocities are parallel and perpendicular to the ambient magnetic field.

Fig. 8*b*. The phase space distributions, $(\zeta, v_{\|B})$ of ions for the same parameters as for Figure 8a.

Fig. 8c. Energy distribution $(v^2 f/2000)$ in arbitrary unit against v/V_a for the same parameters as for Figure 8a.

Fig. 8*d*. The width of pitch angle scattering $< \Theta^*(t) > = (\pi - 2)/2 - c\ \Theta(t) >$ against time for the same parameters as for Figure 8a.

Fig. 9. The velocity distributions of ions observed at $\Omega_i t$ = 200 for MHD turbulence of amplitude, $|\Delta B/B_0|^2$ = 0.5 and θ_{Bk} = 40’, a = 45” for plasma β = 1.0. The velocities are parallel and perpendicular to the ambient magnetic field.

Fig. 10u. The velocity distributions of ions observed at $\Omega_i t$ = 200 for MHD turbulence of amplitude, $|\Delta B/B_0|^2$ = 0.5 and $\theta_{Bk} = 20^\circ$, a = *45°* for plasma β = 1.0. The velocities are parallel and perpendicular to the ambient magnetic field.

Fig. 10b . The average velocity, < v >/VA of ions against root mean square deviation, σ_v */VA* for the same parameters as for Figure 10*a*. The three curves refer to θ_{Bk} = 20”,40”, and 60”.

Fig. 11. The time-averaged pitch angle scattering frequency as a function of injection rate observed at $\Omega_i t$ = 200 for turbulent magnetic fluctuations of amplitude, I $\Delta B/B_0|^2$ = *0.25* and θ_{Bk} = *50”* for plasma β of O(1) and a= 35”, 55*, and 85”.

Fig. 12. The average velocity against root mean square deviation for magnetic fluctuations of amplitude, I $\Delta B/B_0|^2$ =0 .5 and θ_{Bk} =50°, 65”, and 80° for plasma β of O(1) and a = 55”.

B. E. Goldstein, M. Okada, K. M. Srivastava, and B. T, Tsurutani, Jet Propulsion Laboratory, California Institute of Technology, 4800 Oak Grove Drive, Pasadena, CA 91109.
V. Sharma, Defense Science Research Organization, Institute for Systems Studies and Analyses, Metcalf House, Delhi, India.

(Received March 4, 1993;
revised June 11, 1993;
accepted June 11, 1993,)

Paper number 93 JA01748.
0148 -0227/93/JA-01748 $05.00

SRIVASTAVA ET AL.; ACCELERATION OF COMETARY H_20 GROUP PICKUP IONS

SRIVASTAVA ET AL,; ACCELERATION OF COMETARY H_20 GROUP PICKUP IONS

SRIVASTAVA ET AL.; ACCELERATION OF COMETARY H_20 GROUP PICKUP IONS

SRIVASTAVA ET AL.; ACCELERATION OF COMETARY H_20 GROUP PICKUP IONS

SRIVASTAVA ET AL.; ACCELERATION OF COMETARY H_20 GROUP PICKUP IONS

SRIVASTAVA ET AL.; ACCELERATION OF COMETARY H_20 GROUP PICKUP IONS

SRIVASTAVA ET AL,; ACCELERATION OF COMETARY H_20 GROUP PICKUP IONS

SRIVASTAVA ET AL,; ACCELERATION OF COMETARY H_20 GROUP PICKUP IONS

SRIVASTAVA ET AL.; ACCELERATION OF COMETARY H_20 GROUP PICKUP IONS

SRIVASTAVA ET AL.; ACCELERATION OF COMETARY H_2O GROUP PICKUP 10NS

SRIVASTAVA ET AL.; ACCELERATION OF COMETARY H_2O GROUP PICKUP IONS

SRIVASTAVA ET AL.; ACCELERATION OF COMETARY H_2O GROUP PICKUP IONS

SRIVASTAVA ET AL.; ACCELERATION OF COMETARY H_2O GROUP PICKUP IONS

SRIVASTAVA ET AL.; ACCELERATION OF COMETARY H_2O GROUP PICKUP IONS

SRIVASTAVA ET AL.; ACCELERATION OF COMETARY H_2O GROUP PICKUP IONS

SRIVASTAVA ET AL.; ACCELERATION OF COMETARY H_2O GROUP PICKUP IONS

SRIVASTAVA ET AL.; ACCELERATION OF COMETARY H_2O GROUP PICKUP IONS

SRIVASTAVA ET AL.; ACCELERATION OF COMETARY H_2O GROUP PICKUP IONS

SRIVASTAVA ET AL,; ACCELERATION OF COMETARY H_2O GROUP PICKUP IONS

SRIVASTAVA ET AL.; ACCELERATION OF COMETARY H_2O GROUP PICKUP IONS

SRIVASTAVA ET AL.; ACCELERATION OF COMETARY H_2O GROUP PICKUP IONS

SRIVASTAVA ET AL.; ACCELERATION OF COMETARY H_2O GROUP PICKUP IONS

SRIVASTAVA ET AL,; ACCELERATION OF COMETARY H_2O GROUP PICKUP IONS

SRIVASTAVA ET AL.; ACCELERATION OF COMETARY H_2O GROUP PICKUP IONS

SRIVASTAVA ET AL.; ACCELERATION OF COMETARY H_2O GROUP PICKUP IONS

SRIVASTAVA ET AL.; ACCELERATION OF COMETARY H_2O GROUP PICKUP IONS

SRIVASTAVA ET AL.; ACCELERATION OF COMETARY H_2O GROUP PICKUP IONS

SRIVASTAVA ET AL.; ACCELERATION OF COMETARY H_2O GROUP PICKUP IONS

SRIVASTAVA ET AL.; ACCELERATION OF COMETARY H_2O GROUP PICKUP IONS

FIGURE CAPTIONS

Fig. la. Schematic diagram of the simulation geometry. The wave propagates along x axis.

Fig. 1*b*. Scattering of particles by obliquely propagating magnetosonic waves. The electric fields due to the wave and bulk motion of the plasma vanish in a frame moving along the magnetic field with velocity $-V_{ph}/\cos(\theta_{Bk})$, where V_{ph} *is* phase velocity of the wave. Scattering of particles conserves their energy in this frame. The point of injection is marked by a cross, and the region of scattering is shown by the shaded shell,

Fig. 2a. The velocity distribution of ions observed at $\Omega_i t$ = 200 for linearly polarized *MS* waves of amplitude, A = 1.0, M_{res} = 18, and θ_{Bk} = 60", a = 45" for plasma β = 1.0. The velocities are parallel and perpendicular to the ambient magnetic field.

Fig. 2*b*. The phase space diagram $(\zeta, v_{\|B})$ of ions for the same parameters as for Figure *2a*.

Fig. 2c. Energy distribution $(v^2 f/2000)$ in arbitrary unit against *v/VA* for the same parameters as for Figure 2*a*.

Fig. 2*d*. The average velocity, < v > /VA of ions as a function of time t^* for the same parameters as for Figure 2*a*. The three curves refer to θ_{Bk} = 20^s, 40°, and 60°.

Fig. 3a. The velocity of ions observed at $\Omega_i t$ = 200 for circularly polarized *MS* waves of amplitude, A = 1.0 and θ_{Bk} =60" , a = 45" for plasma/3= 1.0. The velocities are parallel and perpendicular to the ambient magnetic field.

Fig. *3b. The* phase space diagram $(\zeta, v_{\|B})$ of ions for the same parameters as for Figure *3a*.

Fig. 3c. Energy distribution $(v^2 f/2000)$ in arbitrary unit against *v/VA* for the same parameters as for Figure 3*a*.

Fig. *3d*. The width of pitch angle scattering < #(t)> = $(\pi - 2)/2$ - < $\Theta(t)$ > against time for the same parameters as for Figure *3a*.

Fig. 4. The velocity distribution of ions observed at flit= 200 for circularly polarized *MS* w aves of amplitude, A = 1.0 and θ_{Bk} =40°, a = 45" for plasma β = 1.0, The velocities are parallel and perpendicular to the ambient magnetic field.

Fig. 5*a*. The velocity distribution of ions observed at $\Omega_i t$ = 200 for circularly polarized *MS* waves of amplitude, A = 1.0 and θ_{Bk} = 20°, α = 45" for plasma β = 1.0. The velocities are parallel and perpendicular to the ambient magnetic field.

Fig. 5*b*. *The* average velocity of ions against root mean square deviation for the same parameters as for Figure 5*a*. The three curves refer to θ_{Bk} = 20",40", and 60°.

Fig. 6. The average velocity, < v >/VA against root mean square deviation, σ_v /VA for circularly polarized *MS* waves of amplitude, A = 0.5 and θ_{Bk} = 50", 65°, 80", a = 55",

Fig. 7. The time averaged pitch angle scattering frequency as a function of injection rate observed at $\Omega_i t$ = 200 for circularly polarized MS wave of amplitude, A = 0.5 and θ_{Bk} = 30', 50", 65", and 80" for plasma b of O(1) and a = 35',55", and 85".

Fig. 8a. The velocity distribution of ions observed at $\Omega_i t$ = 200 for MHD turbulence generated by circularly polarized *MS* waves of amplitude, $|\Delta B/B_0|^2$ = 0.5 and θ_{Bk} =60", a = 45' for plasma β= 1.0. The velocities are parallel and perpendicular to the ambient magnetic field.

Fig. *8b. The* phase apace distribution, $(\zeta, v_{\|B})$ of ions for the same parameters as for Figure 8*a*.

Fig. 8c. Energy distribution $(v^2 f/2000)$ in arbitrary unit against v/V$_a$ for the same parameters as for Figure 8*a*.

Fig. 8*d*. The width of pitch angle scattering < e'(t)> = $(\pi - 2)/2$ -< $\Theta(t)$ > against time for the same parameters as for Figure 8*a*.

Fig. 9. The velocity distributions of ions observed at $\Omega_i t$ = 200 for *MHD* turbulence of amplitude, $|\Delta B/B_0|^2$ = 0.5 and θ_{Bk} = 40", a = 45" for plasma β = 1.0. The velocities are parallel and perpendicular to the ambient magnetic field.

Fig. 10Q. The velocity distributions of ions observed at flit= 200 for *MHD* turbulence of amplitude, $|\Delta B/B_0|^2$ = 0.5 and θ_{Bk} = 20", a = 45" for plasma β = 1.0. The velocities are parallel and perpendicular to the ambient magnetic field.

Fig. 10b . The average velocity, < v >/VA of ions against root mean square deviation, cr$_v$/*VA* for the same parameters as for Figure 10*a*. The three curves refer to θ_{Bk} = 20',40", and 60'.

Fig. 11. ‘f’he time-averaged pitch angle scattering frequency as a function of injection rate observed at $\Omega_i t$ = 200 for turbulent magnetic fluctuations of amplitude, $|\Delta B/B_o|^2$ = 0.25 and θ_{Bk} = 50” for plasma β of O(1) and α = 35”, 55”, and 85”.

Fig. 12. The average velocity against root mean square deviation for magnetic fluctuations of amplitude, $|\Delta B/B_o|^2$ =0.5 and θ_{Bk} =50°, 65”, and 80” for plasma β of O(1) and a = 55”.

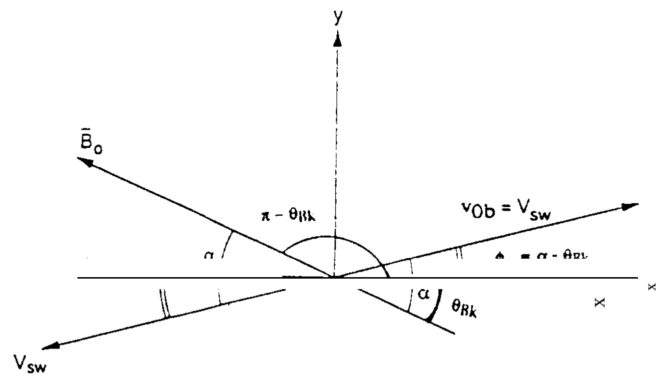

$v_{inj,x} = v_{0b} \cos\phi \quad v_{inj,y} = v_{0b} \sin\phi$

$v_{\parallel B} = -v_x \cos\theta_{Bk} + v_y \sin\theta_{Bk}$

$v_{\perp B} = [(v_x \sin\theta_{Bk} + v_y \cos\theta_{Bk})^2 + (v_z)^2]^{1/2}$

Fig. 1 a

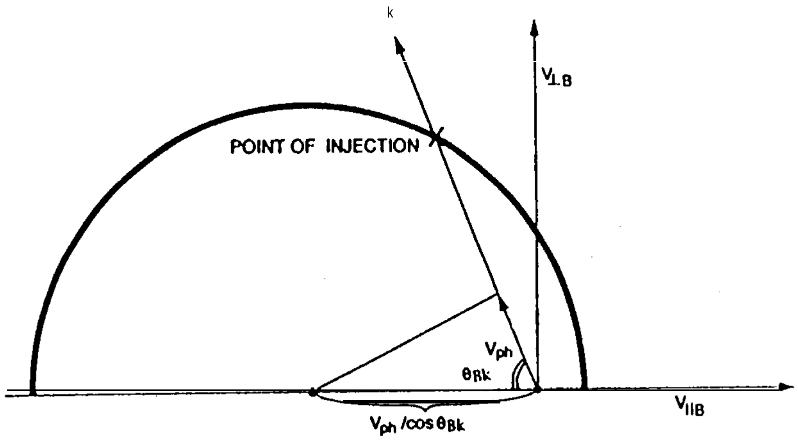

k
$V_{\perp B}$
POINT OF INJECTION
V_{ph}
θ_{Bk}
$V_{ph}/\cos\theta_{Bk}$
$V_{\parallel B}$

Figure 1b.

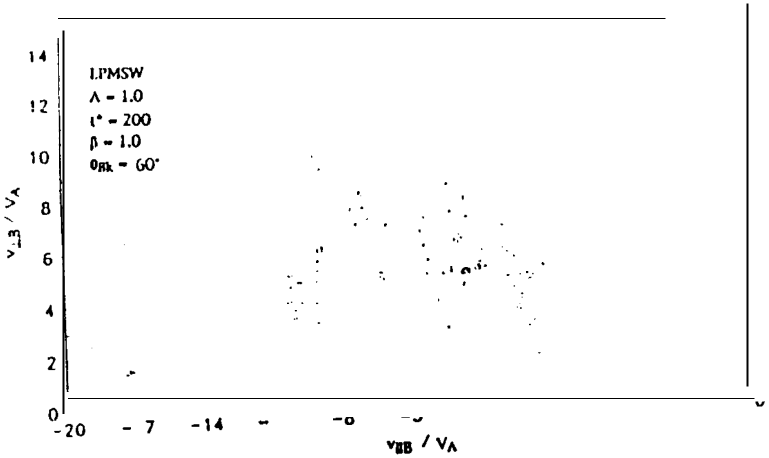

Fig. 2 a

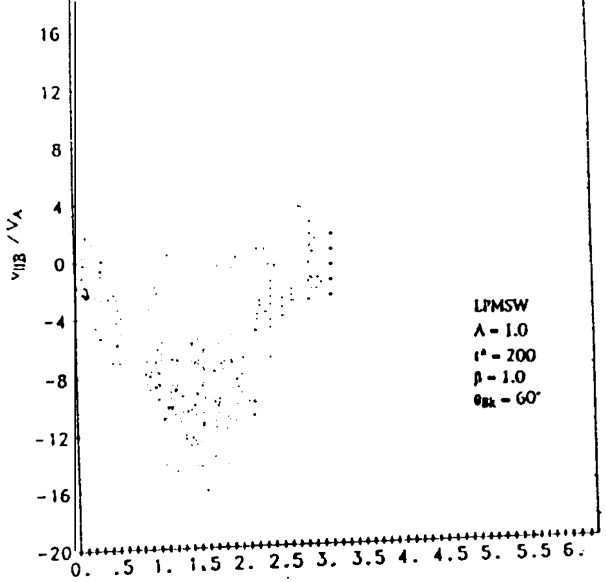

ζ IN RADIANS
Fig. 2 b

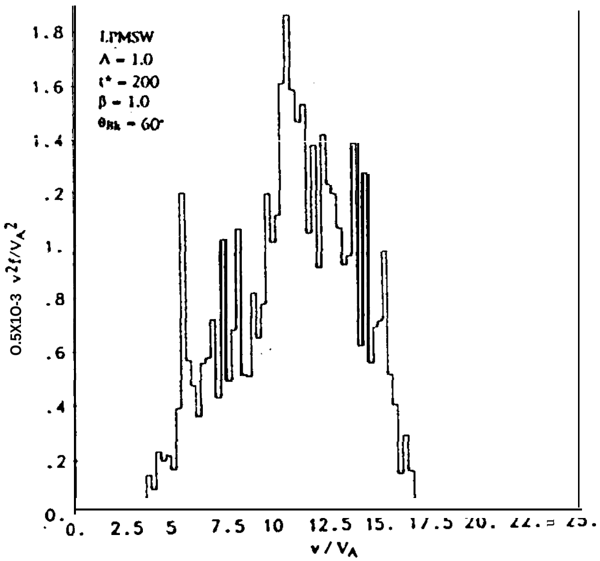

Fig. 2 c

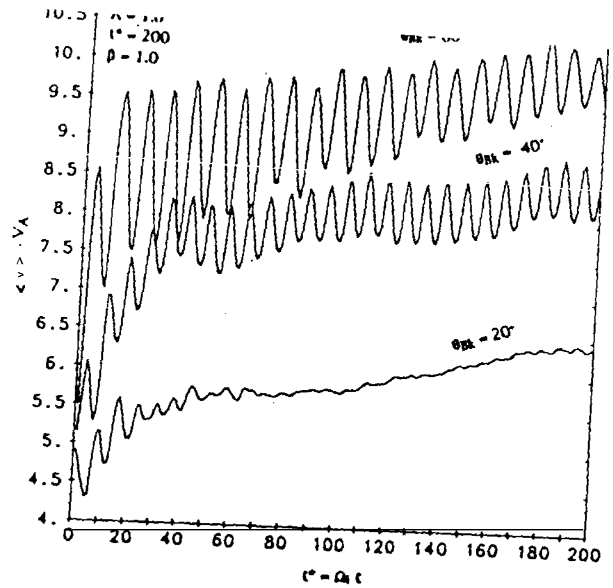

Fig. 2 d

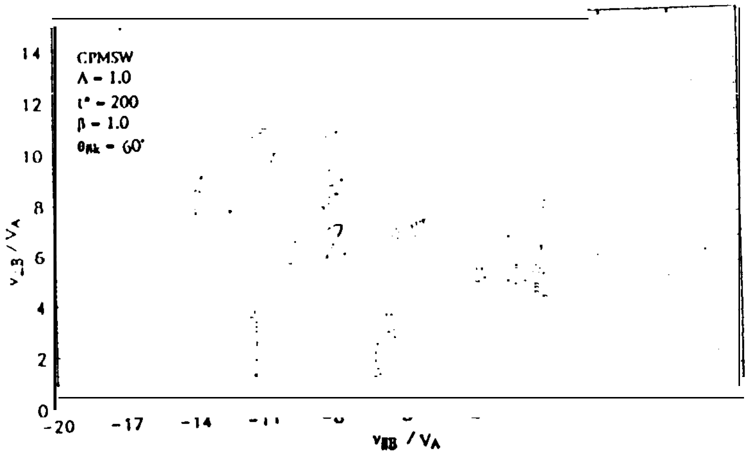

Fig. 3 a

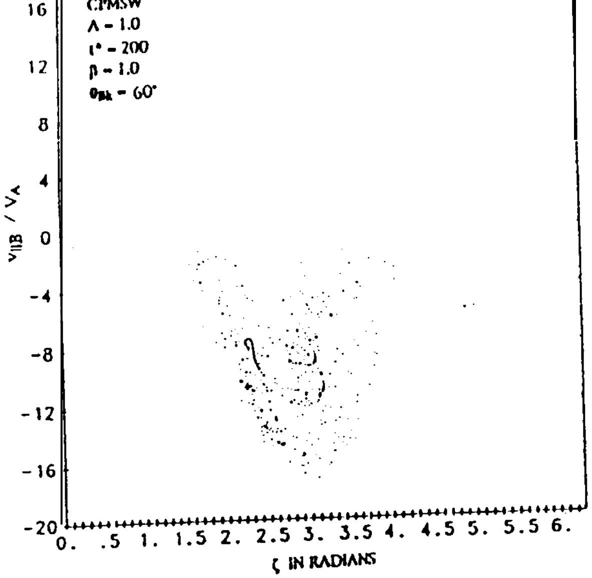
CPMSW
Λ = 1.0
t* = 200
β = 1.0
θBk = 60°
16
12
8
4
0
-4
-8
-12
-16
-20
vIIB / VA
0. .5 1. 1.5 2. 2.5 3. 3.5 4. 4.5 5. 5.5 6.
ζ IN RADIANS

Fig. 3 b

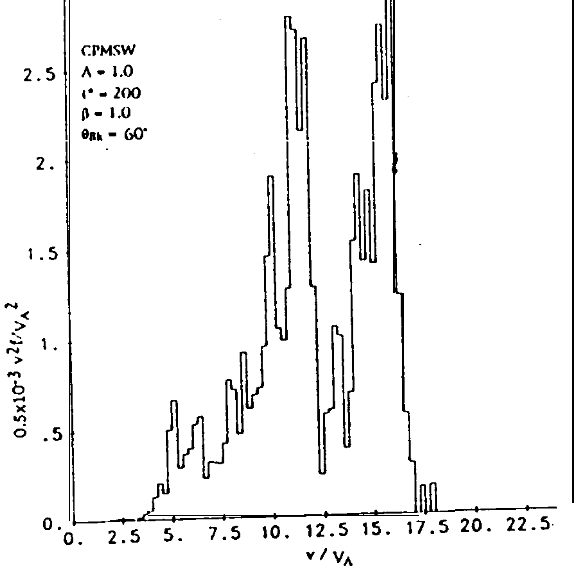

CPMSW
Λ = 1.0
t* = 200
β = 1.0
θBk = 60°
0.5x10-3 v2f/VA2
v / VA
0.
.5
1.
1.5
2.
2.5
0.
2.5
5.
7.5
10.
12.5
15.
17.5
20.
22.5

Fig. 3 c

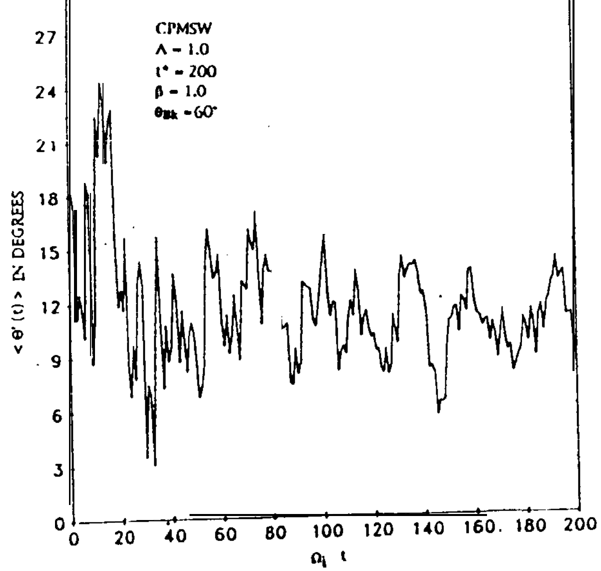

CPMSW
Λ = 1.0
t* = 200
β = 1.0
θBk = 60°
< θ' (t) > IN DEGREES
0
3
6
9
12
15
18
21
24
27
0
20
40
60
80
100
120
140
160
180
200
Ωi t

Fig. 3 d

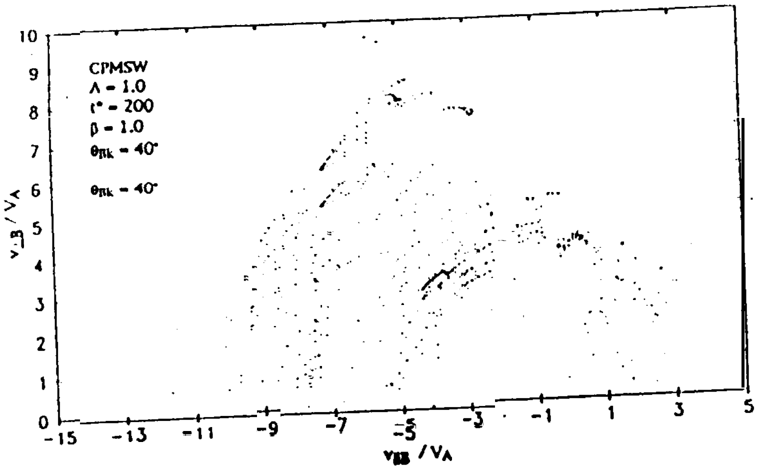
CPMSW
Λ = 1.0
t* = 200
β = 1.0
θBk = 40°
θBk = 40°
10
9
8
7
6
5
4
3
2
1
0
−15
−13
−11
−9
−7
−5
−3
−1
1
3
5

Fig. 4

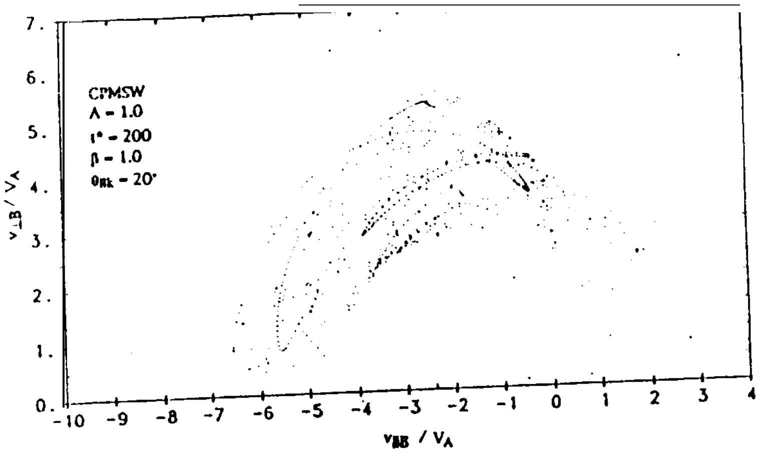
CPMSW
$\Lambda = 1.0$
$t^* = 200$
$\beta = 1.0$
$\theta_{Bk} = 20°$
$v_{\perp B} / V_A$
$v_{\parallel B} / V_A$
0.
1.
2.
3.
4.
5.
6.
7.
-10
-9
-8
-7
-6
-5
-4
-3
-2
-1
0
1
2
3
4

Fig. 5 a

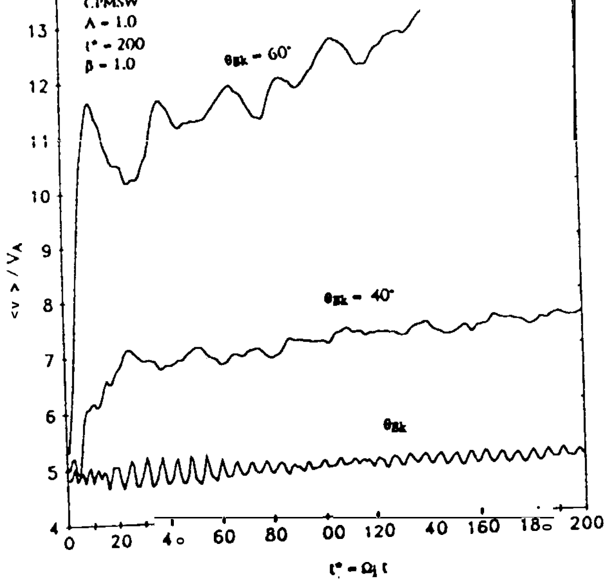

Fig. 5 b

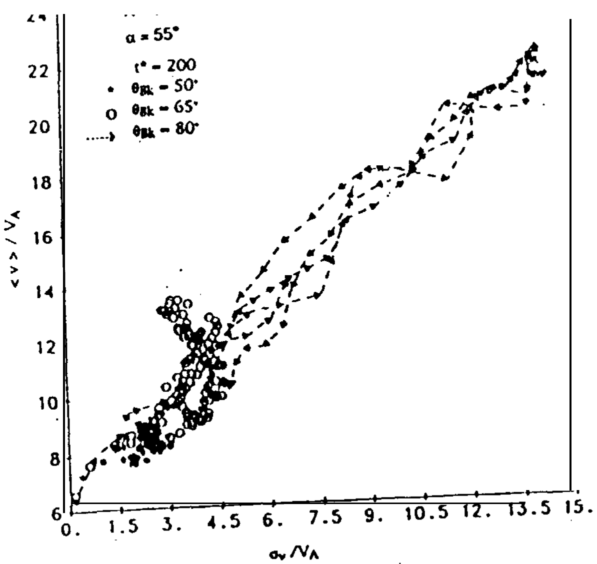

α = 55°
t* = 200
θBk = 50°
θBk = 65°
θBk = 80°
<v> / VA
6
8
10
12
14
16
18
20
22
0.
1.5
3.
4.5
6.
7.5
9.
10.5
12.
13.5
15.
σv /VA

Fig. 6

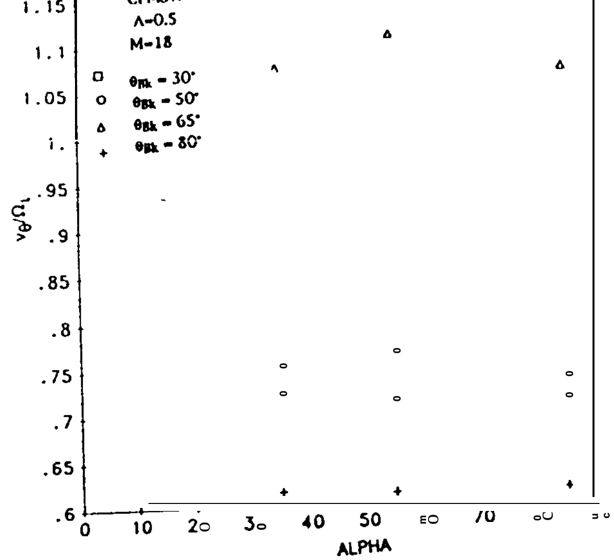
Λ=0.5
M=18
θBk = 30°
θBk = 50°
θBk = 65°
θBk = 80°
vθ/Ωi
1.15
1.1
1.05
1.
.95
.9
.85
.8
.75
.7
.65
.6
0
10
40
50
ALPHA

Fig. 7

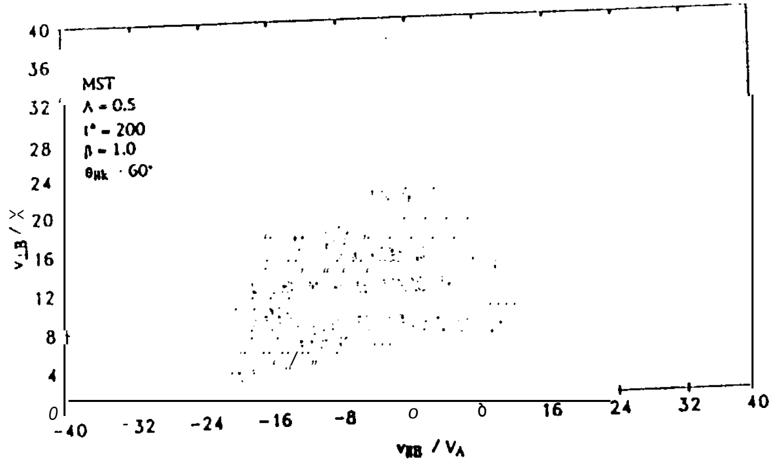
MST
$\Lambda = 0.5$
$t^* = 200$
$\beta = 1.0$
$\theta_{Bk} \cdot 60°$
$v_{\perp B} / V_A$
$v_{\parallel B} / V_A$

Fig. 8 a

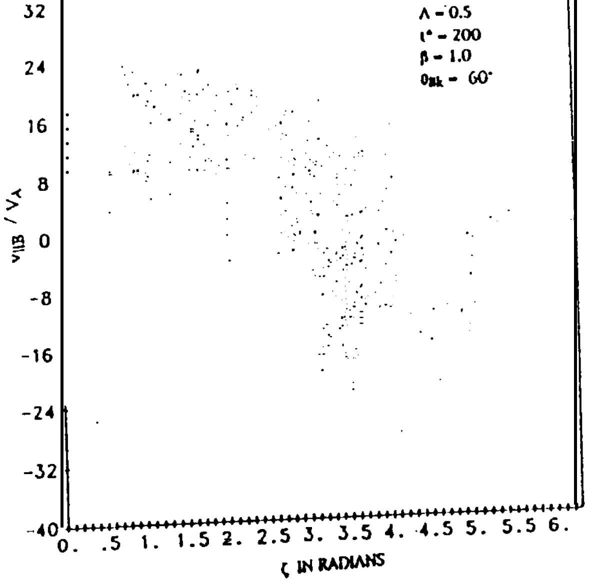
Λ = 0.5
t* = 200
β = 1.0
θBk = 60°
32
24
16
8
0
-8
-16
-24
-32
-40
V∥B / VA
0. .5 1. 1.5 2. 2.5 3. 3.5 4. 4.5 5. 5.5 6.
ζ IN RADIANS
Fig. 8 b

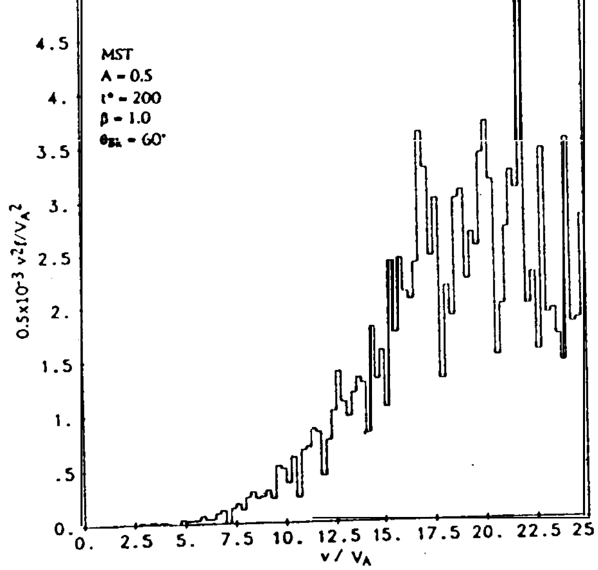
MST
A = 0.5
t* = 200
β = 1.0
θ = 60°
0.5x10-3 v2f/VA2
v / VA
0. 2.5 5. 7.5 10. 12.5 15. 17.5 20. 22.5 25
0. .5 1. 1.5 2. 2.5 3. 3.5 4. 4.5

Fig. 8c

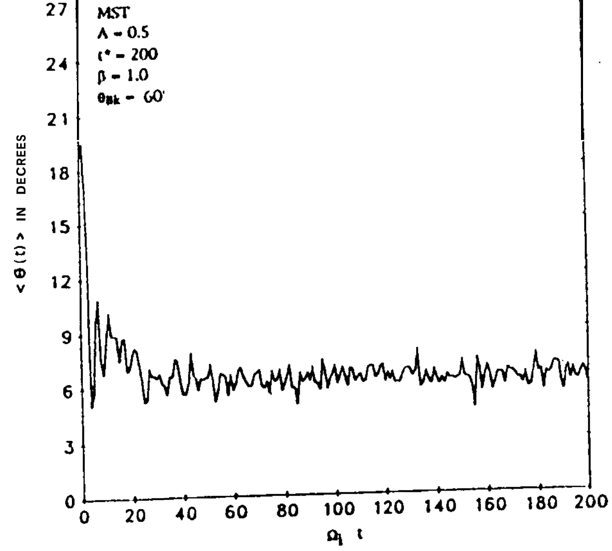
MST
A = 0.5
t* = 200
β = 1.0
θBk = 60°
< θ(t) > IN DECREES
27
24
21
18
15
12
9
6
3
0
0
20
40
60
80
100
120
140
160
180
200
Ωi t

Fig. 8 d

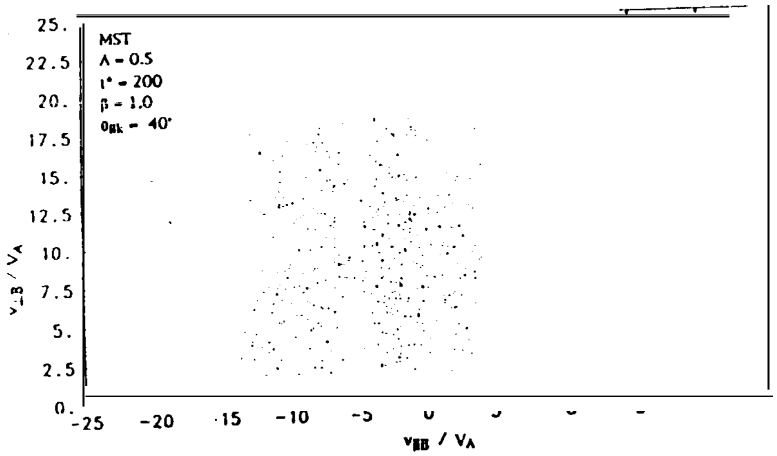
MST
Λ = 0.5
t* = 200
β = 1.0
θ_Bk = 40°
25.
22.5
20.
17.5
15.
12.5
10.
7.5
5.
2.5
0.
v⊥B / VA
-25
-20
-15
-10
-5
0
v∥B / VA

Fig. 9

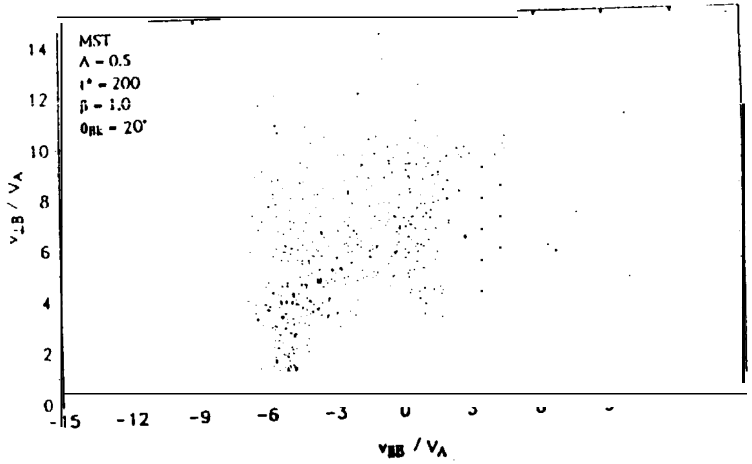

Fig. 10 a

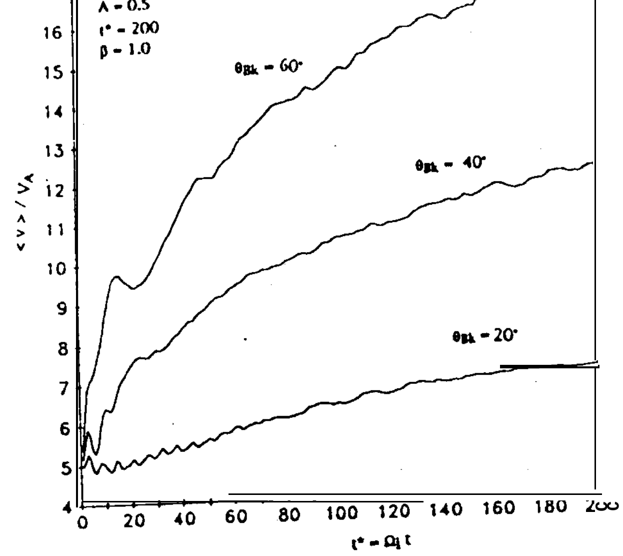

A = 0.5
t* = 200
β = 1.0
θBk = 60°
θBk = 40°
θBk = 20°
<v> / VA
4
5
6
7
8
9
10
11
12
13
14
15
16
0
20
40
60
80
100
120
140
160
180
200
t* = Ωi t

Fig. 10 b

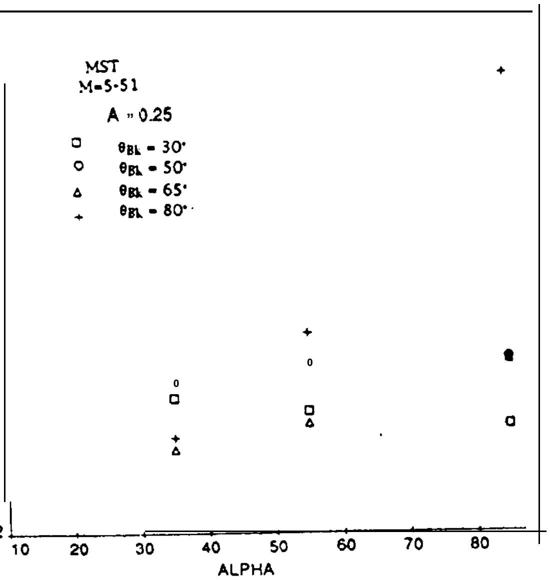

MST
M=5-51
A = 0.25
θ_{BL} = 30°
θ_{BL} = 50°
θ_{BL} = 65°
θ_{BL} = 80°
10
20
30
40
50
60
70
80
ALPHA

Fig. 11

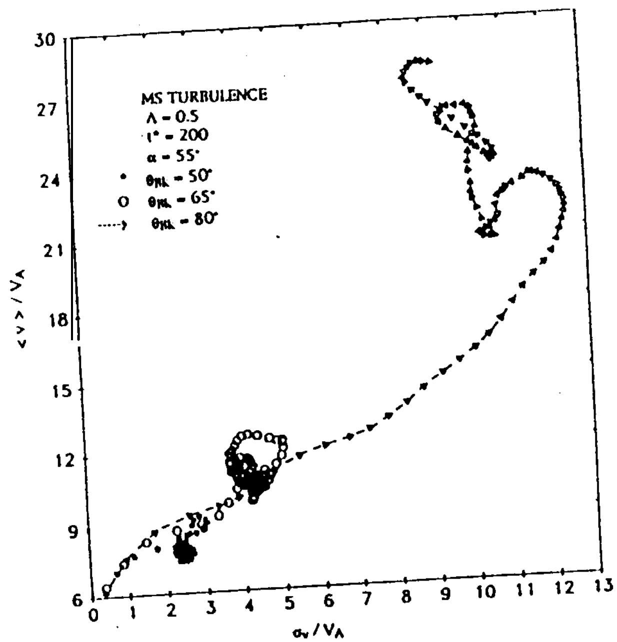

Fig. 12